Thermohydrodynamic modelling of journal bearings under varying load angle and negative groove flow rate

FP Brito, AS Miranda, JCP Claro, JC Teixeira, L Costa and M Fillon

Proceedings of the Institution of Mechanical Engineers, Part J: Journal of Engineering Tribology 2014 228: 955 originally published online 14 March 2014
DOI: 10.1177/1350650114526388

Special Issue Article

Institution of MECHANICAL ENGINEERS
Journal of ENGINEERING TRIBOLOGY

Proc IMechE Part J:
J Engineering Tribology
2014, Vol. 228(9) 955–973

DOI: 10.1177/1350650114526388
pij.sagepub.com
SAGE

Thermohydrodynamic modelling of journal bearings under varying load angle and negative groove flow rate

FP Brito[1], AS Miranda[1], JCP Claro[1], JC Teixeira[1], L Costa[2] and M Fillon[3]

Abstract

The performance of hydrodynamic journal bearings is affected by the conditions under which the lubricant is fed to the bearing gap. Axial grooves are often used and, depending on their location relatively to the load line, they might substantially interfere with the hydrodynamic pressure generation and the thermal behaviour of the bearing. However, many of the existing tools for predicting bearing performance are not able to suitably predict bearing behaviour under varying load angle given the oversimplified way under which they treat lubricant feeding conditions. The present work proposes a detailed thermohydrodynamic approach which realistically incorporates these conditions into the bearing analysis. Special care is put on the mass and energy-conserving models of the ruptured film region and on a detailed treatment of lubricant mixing within the vicinity of grooves. This includes the first full modelling of the effect of negative flow rate in a groove, a phenomenon originally described experimentally in detail by the authors in previous publications, and which happens for a broad range of load/groove angles. An extensive investigation on the influence of loading direction on the performance of twin groove journal bearings has been performed. This parameter is found to affect deeply all major performance parameters due to the interference of groove regions in the hydrodynamic pressure generation and in the flow rates at each groove.

Keywords

Journal bearings, thermohydrodynamic model, groove mixing, load angle, groove angle, axial groove, lubricant feeding conditions, hydrodynamic lubrication, thermal behaviour, bearing performance

Date received: 22 October 2013; accepted: 3 February 2014

Introduction

Frequently, the lubricant supplied to hydrodynamic journal bearings is fed at a prescribed pressure through two diametrically opposed axial grooves, normally located at $\pm 90^{\circ}$ to the load line. The conditions under which the lubricant is fed to the bearing through these grooves, namely lubricant feeding pressure, feeding temperature, number and location of grooves and their actual geometry, significantly affect the bearing behaviour, as highlighted in other works by the authors, both theoretically[1–3] and experimentally.[4–9] However, incorporating these parameters into analyses poses some theoretical difficulties. Namely, a mass-conservative model must be used, with a suitable estimation of the film rupture and reformation boundaries.[10,11] A frequent simplification is to consider that film reformation will occur at the maximum film thickness position or at the groove edges.[12] However, to conveniently evaluate the role of feeding grooves in the behaviour of the bearing it is vital that the real groove dimensions be taken into account.[3] But this will complicate geometry, meshing and algorithm convergence.[10] That is why it is common to use grooves of infinitesimal width (no circumferential extension)[13] or grooves which extend to the full length of the bush body.[14–16] Another commonly used simplification is to use finite sized grooves but imposing flow rate or no feeding pressure (e.g. ambient pressure).[15]

The aforementioned simplifications, which might be suitable in the scope of fast and practical design tools for more conventional and less demanding applications, will be clearly insufficient when severe

[1]Department of Mechanical Engineering, Universidade do Minho, Guimarães, Portugal
[2]Ministry of Energy and Water/DNAAS, Luanda, Angola
[3]Institut Pprime, CNRS – Université de Poitiers – ENSMA, Dept Génie Mécanique et Systèmes Complexes, Futuroscope Chasseneuil, France

Corresponding author:
FP Brito, Department of Mechanical Engineering, Universidade do Minho, Campus de Azurém, 4800-058 Guimarães, Portugal.
Email: francisco@dem.uminho.pt

operating conditions are present.[3] This also applies in situations where a convenient assessment of the role of groove configuration is required, such as cases with variable load angle, where feeding grooves might be located in the vicinity of active bearing regions and interfere with hydrodynamic pressure generation.[9,17]

Also, thermal effects occurring at the groove regions, such as the effect of recirculated hot oil, feeding temperature, reverse flow (oil that re-enters the groove from downstream) or back flow (fresh oil that flows upstream from the groove) are often overlooked due to the simplifications made, although they might often be vital for conveniently assess bearing performance.[18,19] In this scope, the authors assessed the role of each groove on the behaviour of a 50 mm journal bearing with two axial grooves located at $\pm 90^\circ$ to the load line.[6,7] They performed the measurement of the flow rate in each groove (something rarely seen in literature) and found that the cooling effect of each groove strongly depends on the load. Specifically, the downstream groove flow rate grows with increasing eccentricity, while the opposite occurs at the upstream groove.

Under certain combinations of load and speed the hydrodynamic pressure building up in the vicinity of a groove might eventually reverse the direction of the flux of lubricant that was feeding the bearing.[6,7] Under varying loading direction this phenomenon might occur even with lightly loaded bearings.[9] Under these conditions, a portion of the lubricant flowing inside the bearing gap will flow out of the bearing through the groove, which means that the lubricant flow rate at that groove will be negative. Additionally, this hot lubricant will flow along the feeding pipes in reversed direction, mix with the fresh lubricant coming from the feeding pump and effectively raise the temperature of the lubricant fed to the groove with positive flow rate. The first well documented report of these phenomena was made by the authors for heavily loaded journal bearings with diametrically opposed grooves located at $\pm 90^\circ$ with the load line[6,7] and later also under varying loading direction[9] for the same bearing.

To the authors' knowledge, the phenomenon of negative flow rate has rarely been studied in research literature, although some works vaguely refer to this issue.[20] Moreover, this phenomenon is not normally detected in industrial applications because only total flow rate is monitored, at best. Most models for the prediction of bearing behaviour also fail to predict this phenomenon due to the over-simplified way under which the lubricant feeding conditions are treated.[3]

The complexity arising from modelling feeding conditions in a realistic way and the frequent occurrence of negative flow rate might have been a reason for the small amount of works analyzing the influence of loading direction on the steady state performance of twin groove journal bearings.[18,19] Gethin and El-Deihi were among the few researchers addressing this subject. They published a series of experimental and theoretical works with a growing degree of sophistication over time, although focused mainly on high speed bearings.[17,21,22] One of their latter approaches consisted in a more rigorous thermohydrodynamic (THD) approach in comparison to the former works. Unlike previous iterations, viscosity and temperature were allowed to vary along the thickness and heat conduction through the solid bodies was considered. The shaft temperature was imposed as being equal to the mean film temperature, while at the leading edge of the groove the inlet temperature was calculated through a heat balance. The use of such a groove mixing model proved to be determinant for the improvement of the results. With this latter model a much better agreement with experiment was found for the temperature profile. However, huge differences between theory and experiment persisted in flow rate.

Several authors assessed both experimentally[10,4] and theoretically[23,24] the effect of the groove location on the THD performance of steadily loaded journal bearings with one axial groove. In such case, the groove does not substantially interfere with the hydrodynamic pressure profile. It did however affect slightly the performance of the bearings. Roy and Laha[23] and later Roy[24] predicted an optimum location of the groove of around 12° to the load line, in terms of load capacity. The main difference between the two papers is that the former one did not include thermal effects. Apparently, no mass conserving film rupture model has been used in either model. This limitation might not be decisive when dealing with only one single groove, located far from the pressure build-up region (groove angle varied between 0° and 85° to the load line) but it will definitely compromise the validity of the results in the case of twin groove bearings.

Recently, the authors assessed the influence of loading direction on the behaviour of a twin axial groove bearing.[9] The increase of load angle was found to decrease the flow rate at the upstream groove and to increase the flow rate at the downstream groove. Negative flow rate was detected in either groove (although, naturally, never simultaneously) for wide ranges of load. The flow rate trends were found to be strongly dependent on the proximity of grooves to the pressure build-up zones.

An original experimental comparison on the performance of a single ($+90^\circ$ to the load line) and a twin ($\pm 90^\circ$) axial groove journal bearing was also performed by the authors.[8] It was found that, when compared with the single groove arrangement, the twin groove configuration might deprecate the bearing performance under heavily loaded conditions, namely due to uneven lubricant feeding through each groove. It was concluded that bearing performance could be improved under specific regimes by

implementing groove deactivation or flow balancing strategies based on the knowledge of the feeding flow rates through each groove.

From the above analysis and from the findings of previous related works by the group it may be concluded that the phenomena taking place in the vicinity of feeding grooves and their role in bearing performance, particularly when they interfere with hydrodynamic pressure generation, are still not satisfactorily incorporated into most existing bearing performance simulation tools. Also, the assessment of the influence of loading direction on the performance of twin axial groove hydrodynamic journal bearings still needs to incorporate feeding conditions (namely groove geometry) in a convenient manner. Finally, the phenomenon of negative flow rate, which is heavily present in a broad range of load angles, and the associated hot lubricant feedback to the opposite groove, has still not been addressed by existing models and needs to be modelled conveniently.

In the present work, the authors propose a THD model to address the aforementioned issues, with a special attention to the treatment of the phenomena taking place within the grooves and in their vicinity, as well as in the ruptured film region. This model has already been presented in a very recent publication[3] and used to assess the effect that lubricant feeding pressure and temperature, groove length ratio, groove width ratio and groove number (single/twin) have on bearing performance. The results, which were obtained for a broad range of conditions, were found to be in fairly good agreement with experimental published results. They confirmed that indeed lubricant feeding conditions often play vital role in bearing performance and that a careful tuning of the feeding conditions may indeed improve bearing performance. The present work provides a general, complementary description of the model and details some of its unpublished specificities, especially those related to the issue under study, which is the assessment of the influence of load angle on bearing behaviour and the assessment of related phenomena, such as the occurrence of negative feeding flow rate in a groove.

The study now performed may also serve to confirm the robustness of the model, since a broad variation of parameters takes place, with some severe operating conditions occurring: strong pressure and temperature gradients, often in the vicinity of grooves, strong reverse and back flow, hot oil reflux at one of the grooves, unusual film rupture and reformation boundaries, unusual pressure and temperature profiles are likely to occur.

Theoretical model

The present model has been developed based on previous work by the group, both of isoviscous[1] and THD nature.[2] Many of the modelling details have been already provided in those works and also in a very recent paper by the group focusing on the assessment of the influence of lubricant feeding conditions on bearing behaviour,[3] so the present paper provides information which is complementary to those works. Other model specificities, such as the detailed domain normalization and corresponding non-dimensional variables and groups, as well as the particular mathematical expressions used for the boundary conditions may be found in Brito's study.[25]

The model relies on the solution of the THD problem with a special care being put on the realistic treatment of lubricant feeding conditions, namely lubricant feeding pressure, feeding temperature, the actual groove dimensions and their location in relation to the load line (here called load angle or groove angle, Γ).

The model is expected to estimate the main performance parameters relevant for bearing design and performance analysis, such as the hydrodynamic pressure and temperature profiles, minimum film thickness, oil flow rate, shaft locus and power loss, based on inputs such as the operating conditions, the geometric configuration of the bearing and the lubricant feeding conditions.

The basic geometry of a twin groove hydrodynamic journal bearing is presented in Figure 1 with the corresponding axis system. The lubricant is supplied to the bearing at a constant feeding pressure (P_f) and feeding temperature (T_f), through two diametrically opposed axial grooves, located at an angle Γ with the load line (90° in the case of the figure).

The fluid domain is the unwrapped bearing geometry represented in Figure 2(a), which has suffered a coordinate transformation into the normalized reference domain represented in Figure 2(b), considering the assumption that bearing curvature and inertial effects may be neglected.

The coordinate system of the rectangular reference domain is obtained through a variable transformation:

$$x = R_i\alpha; \quad y = h\eta = \bar{h}(\alpha)c_r\eta; \quad z = b\zeta;$$
$$\bar{h}(\alpha) = 1 + \varepsilon\cos(\underbrace{\alpha + \Gamma - \phi}_{\gamma}) \tag{1}$$

Pressure and velocity fields

Concerning the pressure and flow calculations, some of the assumptions made include: the consideration of a steady state regime; thin film approximation, meaning that pressure is considered to be constant across the film thickness (not valid within groove regions); laminar flow, with fluid inertia and gravity effects being negligible when compared with viscous effects; fluid is Newtonian and incompressible, with lubricant viscosity depending solely on temperature; negligible effect of the bearing curvature (small clearance when

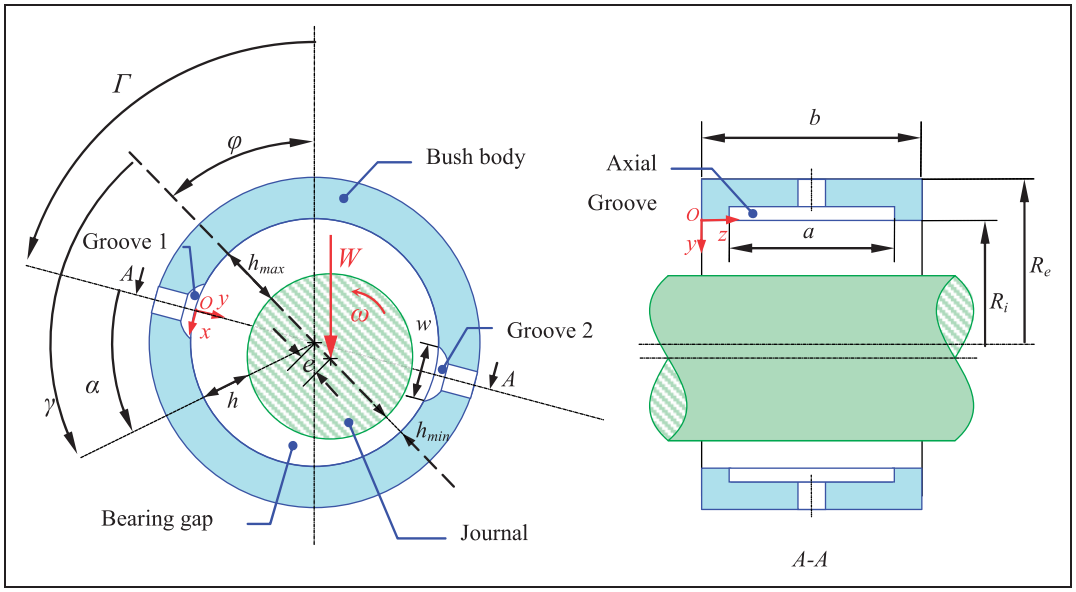

Figure 1. Outline of the bearing geometry.

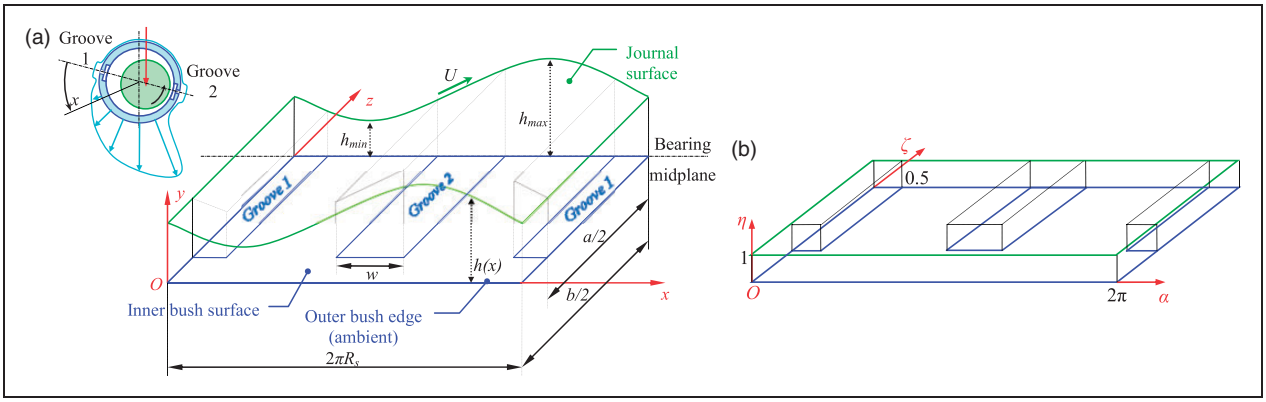

Figure 2. Unwrapped dimensional (a) and non-dimensional (normalized) fluid domain (b).

compared with the bearing radius); absence of contact between surfaces and surface roughness effects (hydraulically smooth surface in the fully hydrodynamic regime); uniform thermal expansion suffered by the components, based on their average temperature (only their diameter is affected – i.e. differential thermal expansion approach).

The Generalized Reynolds Equation (GRE) governs the hydrodynamic pressure field, $P(x,z)$, within the full film region (by itself it is not valid in the ruptured film region). It is derived from a balance of drag-driven and pressure-driven flow rates:[26]

$$\underbrace{\frac{\partial}{\partial x}\left[\rho_l F_2 \frac{\partial P}{\partial x}\right]}_{\substack{\text{Due to circumferential}\\ \text{Poiseulle flow}\\ \text{(pressure driven)}}} + \underbrace{\frac{\partial}{\partial z}\left[\rho_l F_2 \frac{\partial P}{\partial z}\right]}_{\substack{\text{Due to axial}\\ \text{Poiseulle flow}\\ \text{(pressure driven)}}} = \underbrace{U\frac{\partial}{\partial x}[\rho_l h F_3]}_{\substack{\text{Due to circumferential}\\ \text{Couette flow}\\ \text{(drag driven)}}} \qquad (2)$$

Or, in the normalized domain:

$$\frac{\partial}{\partial \alpha}\left[\overline{h}^3 \overline{F_2}\frac{\partial \overline{p}}{\partial \alpha}\right] + \left(\frac{R_i}{b}\right)^2 \frac{\partial}{\partial \zeta}\left[\overline{h}^3 \overline{F_2}\frac{\partial \overline{p}}{\partial \zeta}\right] = \frac{\partial}{\partial \alpha}\left(\overline{hF_3}\right) \qquad (3)$$

The viscosity integrals account for cross-film viscosity variation and are defined as follows:

$$F_0 = \int_0^h \frac{1}{\mu_l}\mathrm{d}y; \quad F_1 = \int_0^h \frac{y}{\mu_l}\mathrm{d}y;$$
$$F_2 = \int_0^h \frac{y}{\mu_l}\left(y - \frac{F_1}{F_0}\right)\mathrm{d}y; \quad F_3 = 1 - \frac{F_1}{hF_0} \qquad (4)$$

However, if the ruptured film region is considered to be at a uniform pressure (ambient), then the flow will be purely drag-driven, and it will be possible to reformulate the expressions of the balance so that the resulting equation may become valid for the whole domain, including the ruptured film region, as

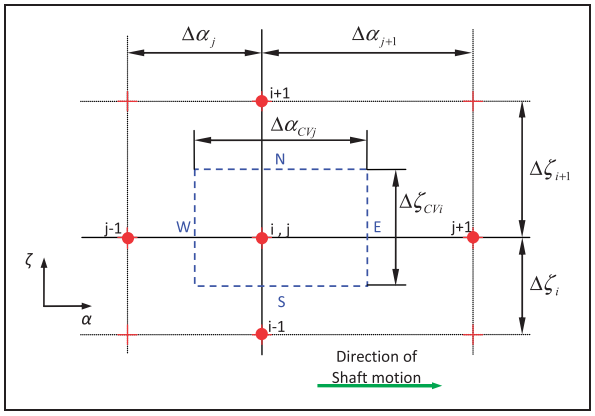

Figure 3. Elementary cell for an arbitrary node of an arbitrary rectangular mesh.

proposed by Elrod[27] and later adapted to the THD case by Costa et al.[2] Firstly, control volumes around each computational node (as depicted in Figure 3) are defined and finite difference expressions for the calculation of Poiseuille and Couette flows at each one of the faces of each control volume are derived. These expressions can be found in Costa et al.[2] or Brito's study.[25]

Then a mass balance to each control volume is carried out:

$$\bar{Q}_\alpha\big|^{E}_{\text{Cou+Poi}} - \bar{Q}_\alpha\big|^{W}_{\text{Cou+Poi}} + \bar{Q}_\zeta\big|^{N}_{\text{Cou+Poi}} - \bar{Q}_\zeta\big|^{S}_{\text{Cou+Poi}} = 0 \tag{5}$$

The result of this equation will be a Reynolds-type finite difference equation which is mass-conservative and valid throughout the whole domain. Through the introduction of a constant β, a switch function g (which is 1 at the full film region and 0 elsewhere) and a new variable θ, a variable substitution for the pressure field is carried out (the pressure at the ruptured film region is considered to be zero, that is, ambient):

$$\bar{p} = g\bar{\beta}(\theta - 1) \tag{6}$$

While θ is defined throughout the whole domain, it will change its character whether within the full film or the ruptured film region. Within the full film region θ is related to pressure: it is simply a substitution variable which is proportional to the local pressure, with β being the constant of proportionality. Within the ruptured film region the pressure is zero (ambient) and θ represents the liquid fraction. It can vary between 0 (the limit case of no lubricant present within the gap, only the gaseous phase present) and 1 (full film at atmospheric pressure, with no gaseous phase present within the gap). The switch function g is responsible for changing the character of θ in each region. The equation is solved to obtain the θ field by the Gauss-Seidel method with under relaxation (to prevent instability). During the iterative process the switch function g simply needs to be updated in every node after each iteration. Once convergence has been achieved, the pressure field is obtained directly from the θ field through equation (6).

An advantage of this method is that it automatically provides the mass flow rates of lubricant crossing all faces of each computation cell and the corresponding local liquid fraction at the ruptured film region. This is very suitable for computing flow rates in places such as groove edges (something vital for incorporating feeding conditions) and for use in ruptured film region thermal models based on effective length (EL) concepts such as those described in a study by Knight and Ghadimi[14] or the one proposed in this work.

The velocity field affects the convective and the dissipative terms of the energy equation so it must also be computed. The expressions for the circumferential and axial components of the velocity are the sum of the Poiseuille and Couette components for variable viscosity:[26]

$$\begin{cases} u_x = \dfrac{\partial p}{\partial x}\left(F_4 - \dfrac{F_1 F_5}{F_0}\right) + U\dfrac{F_5}{F_0} \\ u_z = \dfrac{\partial p}{\partial z}\left(F_4 - \dfrac{F_1 F_5}{F_0}\right) \end{cases} \quad \text{with} \quad \begin{cases} F_4 = \displaystyle\int_0^y \frac{\lambda}{\mu_l}\mathrm{d}\lambda \\ F_5 = \displaystyle\int_0^y \frac{1}{\mu_l}\mathrm{d}\lambda \end{cases} \tag{7}$$

being λ a dummy variable of y. The radial velocity u_y is important as it is responsible for improving heat convection from the fluid to the bush and journal surfaces. It is obtained from the solution of the flow continuity equation, computed solely for the liquid portion of the flow, so it must be affected by the local liquid fraction, θ':

$$\frac{\partial(\theta' u_x)}{\partial x} + \frac{\partial(\theta' u_y)}{\partial y} + \frac{\partial(\theta' u_z)}{\partial z} = 0; \quad \theta' = \min(1;\theta) \tag{8}$$

Hence, the non-dimensional radial velocity $\bar{u}_y$ can be obtained by integrating the following equation along η:

$$\frac{\partial(\theta'\bar{u}_x)}{\partial\alpha} - \frac{\eta}{\bar{h}}\frac{\partial\bar{h}}{\partial\alpha}\frac{\partial(\theta'\bar{u}_x)}{\partial\eta} + \frac{1}{\bar{h}}\frac{\partial(\theta'\bar{u}_y)}{\partial\eta} + \frac{R_i}{b}\frac{\partial(\theta'\bar{u}_z)}{\partial\zeta} = 0 \tag{9}$$

And the boundary conditions will be the no penetration conditions at the walls, which can be written in the normalized velocities of the reference domain or the non-dimensional velocities:[25]

$$\begin{cases} \bar{\eta} = 0 \quad \text{for} \quad \eta = 0 \\ \bar{\eta} = 0 \quad \text{for} \quad \eta = 1 \end{cases} \quad \text{or} \quad \begin{cases} \bar{u}_y = 0 \quad \text{for} \quad \eta = 0 \\ \bar{u}_y = \dfrac{\partial\bar{h}}{\partial\alpha} \quad \text{for} \quad \eta = 1 \end{cases} \tag{10}$$

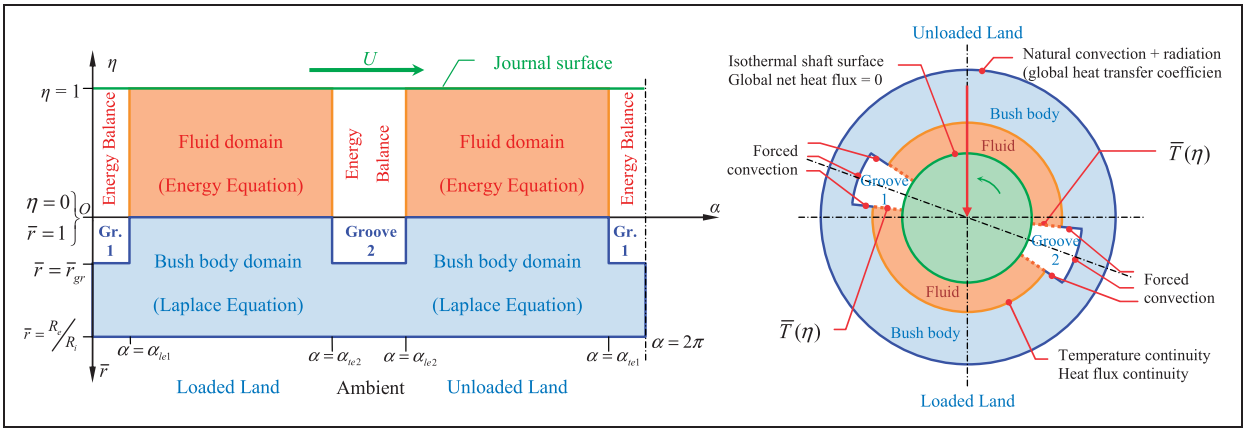

Figure 4. Outline of the calculation domains and boundary conditions used in the thermal model.

The lubricant feeding flow rate is obtained through a mass balance of the liquid phase crossing the boundaries which define the groove region. Most flow rates are obtained from those used in the control volume method. Some others (e.g. backflow and reverse flow) need to be obtained by integrating the corresponding negative portion of the velocity profile at the groove boundaries, affected by the liquid fraction.

Thermal model

The reference domains at which thermal calculations are carried out are schematically represented in Figure 4 both in unwrapped and wrapped form. The unwrapped bush body domain is represented in the non-dimensional cylindrical coordinate system $(O_r, \bar{\bar{r}}, \bar{\alpha}, \bar{\bar{\zeta}})$. Basically, three calculation domains are depicted in Figure 4: the fluid domain, where the energy equation is solved; the bush body domain, where the Laplace equation, which governs conductive heat transfer, is solved; the groove regions, where the Reynolds equation is not applicable (thin film condition is not valid). In this latter domain no velocity field is calculated and therefore only mass and energy balances are performed.

The various domain interfaces are dealt with specific boundary conditions, as depicted in Figure 4. They are detailed further ahead. As simplifying assumptions it was assumed that axial temperature gradients are negligible (thermal calculations are performed in the midplane only); although this is generally a good approximation,[28–30] nonetheless, a novel model was proposed for the vicinity of grooves (where relevant axial gradients might be present); the heat transfer is dominated by the convective terms, except in the radial direction (where diffusive terms are relevant), therefore the circumferential and axial diffusive terms may be neglected when compared with the corresponding convective terms (conductive heat transfer is purely radial);[26,31] only dissipative terms based on transverse gradients are relevant;[26] the bearing is perfectly aligned, i.e. axial symmetry is assumed.

Fluid domain. The following simplified form of the energy equation, for the full film region, at the midplane of the bearing may be therefore obtained:[26]

$$\underbrace{\rho c_p\left[u_x\frac{\partial T}{\partial x}+u_y\frac{\partial T}{\partial y}\right]}_{\text{convective term (convection)}} = \underbrace{K\frac{\partial^2 T}{\partial y^2}}_{\text{diffusive term (conduction)}} + \underbrace{\mu\left(\frac{\partial u_x}{\partial y}\right)^2}_{\substack{\text{dissipative term}\\ \text{(heat generation)}}} \tag{11}$$

Equation (11) is valid for the full film region, with ρ, c_p, K and μ corresponding to the lubricant's local properties (density, specific heat, thermal conductivity and dynamic viscosity). But it is possible to extend the validity of the energy equation to the ruptured film region, which has dual flow (lubricant and gaseous streamers) if an approach based on an EL concept[14] is used. The EL concept relies on the consideration that the liquid lubricant occupies only a fraction of the bearing length, the so-called EL of lubricant. The fraction of the bearing length filled with liquid lubricant can be obtained from the integration of the liquid fraction, θ', provided by the Elrod Algorithm:

$$\overline{EL} = 2\int_0^{1/2}\theta'\,\mathrm{d}\zeta \quad \text{with} \quad \theta' = \min(1,\theta) \tag{12}$$

Assuming as simplification that no heat exchange exists between the liquid and the gaseous streamers (no axial heat flow) and that both phases share the same temperature and velocity fields, then the heat transfer and viscous dissipation phenomena will occur in parallel at each medium and the total convective, dissipative and diffusive terms of equation (11) will be the sum of the partial terms of each

phase. For instance, the convective term will be the following:

$$\overline{EL}\cdot\rho_l c_{pl}\left[u_x\frac{\partial T}{\partial x}+u_y\frac{\partial T}{\partial y}\right]+\left(1-\overline{EL}\right)\cdot\rho_g C_{pg}\left[u_x\frac{\partial T}{\partial x}+u_y\frac{\partial T}{\partial y}\right]=\left(\rho C_p\right)_{eq}\left[u_x\frac{\partial T}{\partial x}+u_y\frac{\partial T}{\partial y}\right] \tag{13}$$

With the equivalent properties being defined as follows:

$$\left(\rho C_p\right)_{eq}=\overline{EL}\cdot\rho_l c_{pl}+\left(1-\overline{EL}\right)\cdot\rho_g C_{p_g} \tag{14}$$

The same can be done concerning the remaining terms of the energy equation, yielding the following energy equation valid throughout the whole fluid domain, both in dimensional and non-dimensional form:

$$\underbrace{\left(\rho c_p\right)_{eq}\left[u_x\frac{\partial T}{\partial x}+u_y\frac{\partial T}{\partial y}\right]}_{\text{convective term (convection)}}=\underbrace{K_{eq}\frac{\partial^2 T}{\partial y^2}}_{\text{diffusive term (conduction)}}+\underbrace{\mu_{eq}\left(\frac{\partial u_x}{\partial y}\right)^2}_{\substack{\text{dissipative term}\\ \text{(heat generation)}}} \tag{15}$$

$$Pe\left[\bar{u}_x\frac{\partial\bar{T}}{\partial\alpha}+\left(\frac{\bar{u}_y}{\bar{h}}-\frac{\bar{u}_x\eta}{\bar{h}}\frac{\partial\bar{h}}{\partial\alpha}\right)\frac{\partial\bar{T}}{\partial\eta}\right]=\frac{1}{\bar{h}^2}\frac{\partial^2\bar{T}}{\partial\eta^2}+Br\frac{\bar{\mu}_{eq}}{\bar{h}^2}\left(\frac{\partial\bar{u}_x}{\partial\eta}\right)^2 \tag{16}$$

With Pe and Br being the Peclet and the Brinkman numbers, respectively.

It is possible to adapt the EL approach to the experimental evidence that, in reality, a portion of the lubricant adheres to the shaft surface flowing at uniform velocity instead of flowing along streamers under Couette flow.[32,33] This will affect heat transfer since no velocity gradients (and therefore no viscous dissipation) will be present for that portion of the lubricant. Some authors have taken this phenomenon into account,[14] although within the scope of a simplified model. The present model uses a similar approach, already described in detail in a previous publication.[3] With this approach the same equations will be used, but the resulting equivalent properties at the ruptured region will be calculated diversely and will vary radially, whether within the streamer region or the layer region. It was found that the choice of the fraction of lubricant adhered to the shaft strongly affects the inner bush surface temperature within the unloaded land of the bearing (no viscous dissipation occurs within the shaft-adhered layer, therefore the temperature fade was stronger), while the temperature at the loaded land of the bearing was only marginally affected by this parameter.[25]

The energy equation is solved as an initial value problem in the circumferential direction. If a region with negative speed exists, then a domain separation similar to the one proposed by Boncompain et al.[13] is used. In this iterative approach the calculations are performed successively in the two separate velocity domains (positive and negative) as initial value problems and in the direction of the flow. The results of one domain will supply the boundary/initial conditions for the next iteration of the other one.

Bush body domain. The Laplace Equation in cylindrical coordinates[26] is used for the solution of the conductive heat transfer across the bush body:

$$\frac{\partial^2\bar{T}_b}{\partial\bar{r}^2}+\frac{1}{\bar{r}}\frac{\partial\bar{T}_b}{\partial\bar{r}}+\frac{1}{\bar{r}^2}\frac{\partial^2\bar{T}_b}{\partial\alpha^2}=0 \tag{17}$$

Using central finite differences the following expression has been obtained, which can be solved with the successive over-relaxation method:

$$\bar{T}_{j,kb}=\frac{\left(\bar{T}_{j,kb+1}-\bar{T}_{j,kc}-1\right)\cdot\left(\frac{1}{2\bar{r}_{kb}\Delta\bar{r}}+\frac{1}{\Delta\bar{r}^2}\right)+\frac{\bar{T}_{j+1,kb}-\bar{T}_{j-1,kb}}{\bar{r}_{kb}\Delta\alpha_j}}{2\left[\left(\frac{1}{\bar{r}_{kc}\Delta\alpha_j}\right)^2+\frac{1}{\Delta\bar{r}^2}\right]} \tag{18}$$

With j and kb being the circumferential and radial indexes of the nodes of the bush body domain, with $\bar{r}={}^{r}/_{R_i}$ being its non-dimensional radial coordinate and with $\Delta\alpha$ and $\Delta\bar{r}$ being the non-dimensional circumferential and radial spacing between the current and the previous node.

Groove regions. The role of lubricant feeding grooves is vital for bearing performance, and this paper, along with other experimental and theoretical ones published by the authors, aims at highlighting this fact. Within these regions the Reynolds equation is no longer valid (the thin film assumption does not apply). Some authors have indeed carried out the CFD modelling of the flow within groove regions for a limited amount of cases,[34,35] but if such calculations would be performed for a broad set of conditions they would require massive computation time.

The approach of the present work consists rather on a detailed mass and energy balance performed to groove regions, incorporating a suitable modelling of groove mixing. The groove region, with the control volume used for the balance and the various intervening heat fluxes is outlined in Figure 5(a).

The aim of the groove balance is to estimate the initial values to be used for the calculation of the temperature field of the fluid domain located downstream

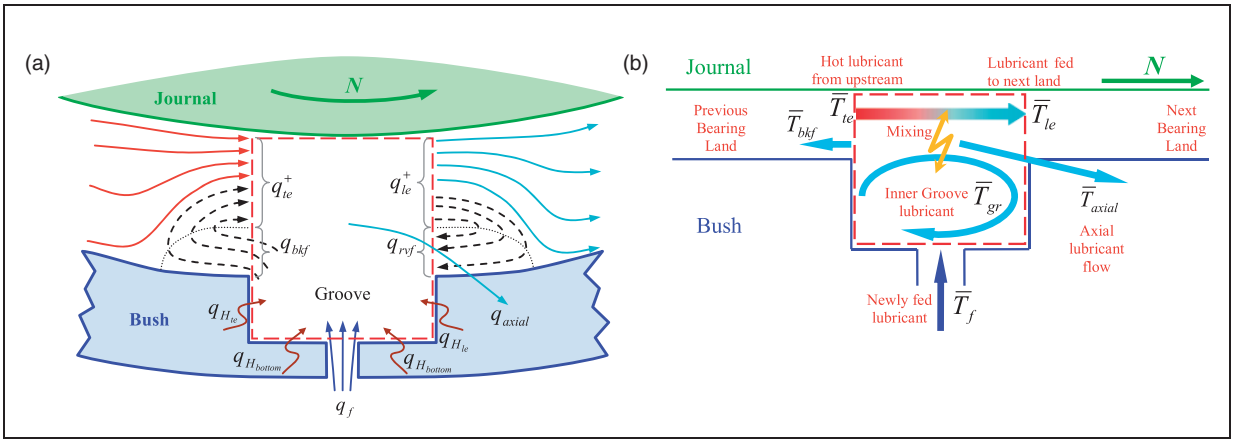

Figure 5. (a) Heat fluxes across the boundaries of the groove region in the presence of back flow upstream and reverse flow downstream of the groove; (b) outline of the thermal mixing model within the groove region.

of the corresponding groove, with an energy conservative approach and without the need for CFD modelling. All major heat fluxes crossing the boundaries of the groove regions have been taken into account:

- heat fluxes due to inbound and outbound lubricant flow, including feeding oil, hot oil carryover coming from upstream, groove oil backflow (upstream of the groove) and reverse flow (coming from downstream of the groove), and even negative feeding flow rate in one of the grooves (hot oil reflux);
- convective heat transfer between the bush body and the inner groove lubricant;
- incorporation of the influence of the groove length ratio, a/b;
- the existence of a non-uniform temperature profile at the inlet section (leading edge of the groove).

The energy balance will provide the total thermal load of all outbound flows. But the thermal load distribution among these several outbound flows leaving the groove may vary. That is, the temperature of each flow may vary depending on the inner groove flow patterns and mixing. This is something that the energy balance cannot predict by itself, given that no flow calculations are performed within grooves. Therefore, the degree of mixing between the various lubricant fluxes and the inner groove lubricant must be modelled. A mixing coefficient, c_{mix}, has been introduced. It varies between 0 (no mix – hot oil coming from upstream does not heat groove oil) and 1 (perfect mix – hot oil coming from upstream perfectly mixes with groove oil).

This mixing model, sketched in Figure 5(b), has already been detailed in a recent publication.[3] It relates the feeding temperature, the inner temperature of the groove, $\bar{T}_{gr}$, the axial flow temperature $\bar{T}_{axial}$ and backflow temperature, $\bar{T}_{bkf}$ in case backflow is present:

$$\bar{T}_{axial} = \bar{T}_{bkf} = \bar{T}_{gr}; \quad \bar{T}_{gr} = c_{\mathrm{mix}}\bar{T}_{le} + (1 - c_{\mathrm{mix}})\bar{T}_f \tag{19}$$

It should be stressed that, unlike other approaches, this mixing coefficient is not used as an alternative to the energy and mass balances (which account for the temperatures and lubricant flow rates crossing the several borders of the groove). All of these flow computations are performed by the present model in an energy-conservative manner. c_{mix} is used solely to differentiate the average temperature of each one of the outbound flows.

The mixing efficiency within a groove will depend on factors such as journal speed, eccentricity and groove geometry. Since the derivation of a physical-backed value is out of the scope of this work, a fixed value of 0.1 was selected after a parametric study. This small mixing coefficient is in agreement with CFD studies,[34] which concluded that the flows occurring within the groove interior are highly recirculating but have almost negligible effects on thermal mixing.

Based on the aforementioned considerations, the energy balance yields the following leading edge temperature:

$$\bar{T}^{+}_{le} = \frac{\bar{q}^{+}_{te} + \bar{q}_H + \bar{Q}_f\bar{T}_f + |\bar{q}_{rvf}| - \left(|\bar{Q}_{axial}| + |\bar{Q}_{bkf}|\right)\cdot(1 - c_{\mathrm{mix}})\bar{T}_f}{c_{mix}|\bar{Q}_{axial}| + c_{mix}|\bar{Q}_{bkf}| + \bar{Q}^{+}_{le}} \quad (\bar{T}_f \geqslant 0) \tag{20}$$

Negative flow rate. The previous calculations were based on the rather common sense notion of a positive feeding flow rate. But in the case of multi groove bearings the feeding flow rate in one of the grooves

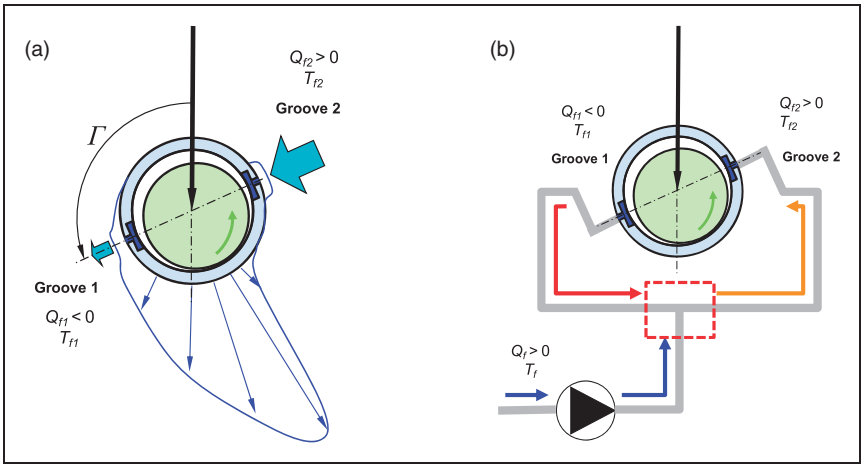

Figure 6. Outline of the mechanism of negative feeding flow rate (a); occurrence of negative flow rate at groove 1 causes an effective rise of the feeding temperature at groove 2 due to mixing of hot oil with fresh oil.

might indeed be negative under certain operating conditions, that is, hot oil flows out of the bearing gap through that groove. This phenomenon has been described experimentally by the authors, both for $\Gamma = 90°$ (grooves located at $\pm 90°$ to the load line)[6,7] as for other load angles.[9] This phenomenon, depicted in Figure 6(a), has been rarely treated or even referenced in literature. To the authors' knowledge, only EI-Deihi and Gethin[17] introduced a slight modification to their model in order to handle this possibility, but in a simplified way.

If negative feeding ($\bar{Q}_{f1} < 0$) occurs at groove 1, then $\bar{T}_{f1}$ is not properly a feeding temperature but it is actually the temperature of the hot oil getting out of the bearing through that groove. While equation (20) still applies under these conditions, some of the temperatures which enter in that balance must be estimated differently. The mixing coefficient, c_{mix}, loses its physical significance in the absence of fresh oil entering the system and the temperature of the outward fluxes will depend solely on the inbound energy flows. These will be the recirculated oil heat transfer rate, $\bar{q}^+_{te}$, and the reverse flow heat transfer rate, $\bar{q}_{rvf}$, if it exists. Under these conditions, it seems reasonable to consider that all outward fluxes will display a temperature similar to the groove temperature, that is:

$$\bar{T}_{f1} = \bar{T}_{gr} = T^+_{le} = \bar{T}_{axial} = \bar{T}_{bkf} \tag{21}$$

Applying these assumptions, equation (20) becomes:

$$\bar{T}^+_{le} = \frac{\bar{q}^+_{te} + \bar{q}_H + |\bar{q}_{rvf}|}{\bar{Q}^+_{le} + |\bar{Q}_{bkf}| + \bar{Q}_{axial} - \bar{Q}_{f1}} \qquad (\bar{Q}_{f1} < 0) \tag{22}$$

There is an additional phenomenon associated with the negative flow rate which, to the authors' knowledge, has never been documented in literature and it is outlined in Figure 6(b): when negative flow rate occurs at one of the grooves, the hot oil flows out of the bearing through that groove, flows backward inside the feeding channels until it mixes with the coming from the feeding pump, heating it. This heated lubricant is then supplied to the other groove, the only with positive flow rate. As a consequence, an effective rise of the feeding temperature at the opposite groove occurs. This curious effect has been documented experimentally in the aforementioned references.

It is possible to incorporate this phenomenon into the analysis by using two different feeding temperatures (one for each groove). If the flow rates are both positive, then they will be both equal to $\bar{T}_f$. Otherwise, a thermal balance must be performed to the control volume represented in Figure 6(b) by the red dotted box.

In the presence of hot oil reflux, for instance at groove 1 (as sketched in Figure 6), the effective feeding temperature at groove 2, $\bar{T}_{f2}$ will be obtained by:

$$\begin{aligned} \bar{T}_{f2} &= \frac{\bar{Q}_f \bar{T}_f - \bar{Q}_{f1} \bar{T}_{f1}}{\bar{Q}_{f2}} \\ &= \frac{(\bar{Q}_{f1} + \bar{Q}_{f2}) \cdot \bar{T}_f - \bar{Q}_{f1} \bar{T}_{f1}}{\bar{Q}_{f2}} \qquad (\bar{Q}_{f1} < 0) \end{aligned} \tag{23}$$

Neglecting this effect will cause an under-prediction of the maximum bush temperature. This phenomenon seems especially important in the presence of varying load angle.

Axial temperature gradient compensation in groove regions. The leading edge temperature, $\bar{T}^+_{le}$, calculated through equations (20) or (22) is representative mainly of what happens along the axial extension of the groove's leading edge and not so much of the whole axial extension of the bearing (also called inlet section). If the groove length is close to the bearing length, then this difference will not be significant. If it is small, then the temperature which may be more

representative of the thermal load of the whole bearing length (the inlet section temperature, $\bar{T}_{is}$) may be estimated by using the knowledge of the 3D velocity field within the non-grooved axial extension of the bearing and performing an energy balance to that region. This methodology has already been proposed by Brito et al.[3]

Conditions at the interfaces. The conditions set at the various interfaces, as already outlined in Figure 4, are presented in continuation.

At the shaft–film interface a condition of no net heat flux was imposed. This may be considered as a midterm between the shaft acting as a heat source (as in the case of a gas-turbine bearing located at the vicinity of the combustion chamber) or as a heat sink (as in the case of a cryogenic pump) for the bearing system. Also, the shaft surface temperature is considered to be constant, following experimental evidence.[36,37] These two assumptions are widely accepted and used in the literature.[38–40]

At the bush–film interface, the temperature and heat flux continuity conditions, which are physically accurate, are applied, while natural and forced convection conditions are used at the bush–ambient interface and at the inner groove walls, respectively. It is worth noting that the accounting for convective heat transfer at the inner groove walls must be done both in the bush body conduction calculation as well as in the groove thermal balance. If convection is computed only in one of these domains, then an artificial heat source/sink will exist in the solution of the problem due to this. A value of 750 $W/m^2 K$ was chosen for H_{gr}. Such high value appears to be in better agreement with the highly recirculating flow found within groove regions.[34,35] It allowed the replication of the strong temperature fade usually observed experimentally in the vicinity of grooves.[5]

Numerical procedure

The present analysis was implemented in FORTRAN 90/95. The global algorithm is outlined in Figure 7.

The selection of the mesh parameters and the convergence criteria was based on a comprehensive parametric study in order to obtain a good compromise between accuracy and processing time. The approach relied on the use of refined meshes in order to detect more subtle phenomena such as reverse flow. Totally, 221 nodes were used circumferentially, 30 axially (half bearing), 35/50 radially (fluid/solid domain). After the first few iterations, the two cells in the vicinity of all groove edges were refined by a factor of six.

Convergence of the θ field near groove edges or oscillating ruptured film boundaries was sometimes difficult to attain, but since this always occurred in only a few cells, cycle exit criteria were carefully defined for these situations. Occasional divergence towards ∞ in θ calculations was avoided by setting upper limits to the variation of θ.

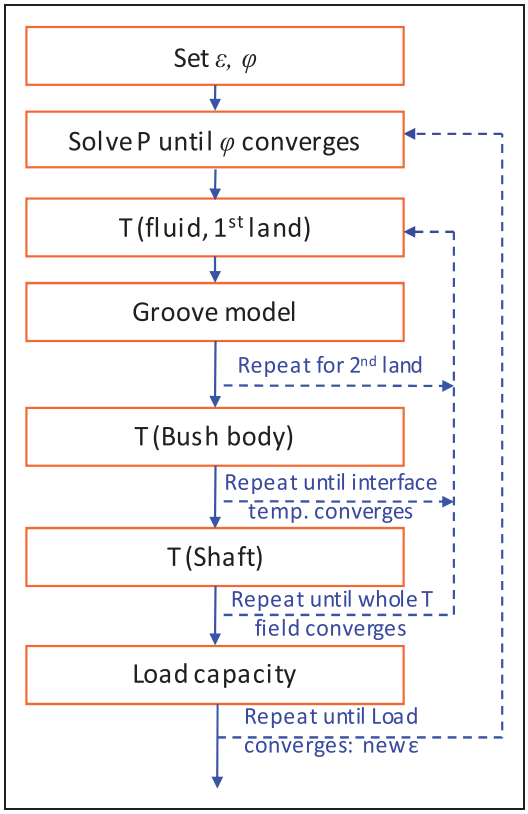

Figure 7. Outline of the main steps of the numerical algorithm.

Taking into account the small randomness found in the results (even at very high eccentricities), along with the small differences found between the results obtained with the selected mesh parameters and the finest meshes tested, the present algorithm seems to be particularly robust.

Model validation

Since there is a lack of models presenting a thorough validation with experimental data, a broad validation of the present model has been performed. Good theoretical–experimental correlation has been observed for reputable results available in the literature,[29] as well as for results from the authors.[5,41] These comparisons have been presented in a previous publication.[3] For the present work it seemed important to complement it with tests for varying load angle. Figure 8 highlights the comparison of the present analysis against experimental data published by the authors for two Γ values (60° and 120°).[9] The first comparison (Figure 8a) refers to flow rate, both total and through each groove, for a load angle of 120°. Although the absolute magnitude of flow rate was underestimated, the trends of the flow rate curves at both grooves are very similar, with the occurrence on negative flow rate in groove 1 having been correctly predicted by the model. Its effect on the temperature rise of the feeding lubricant and at

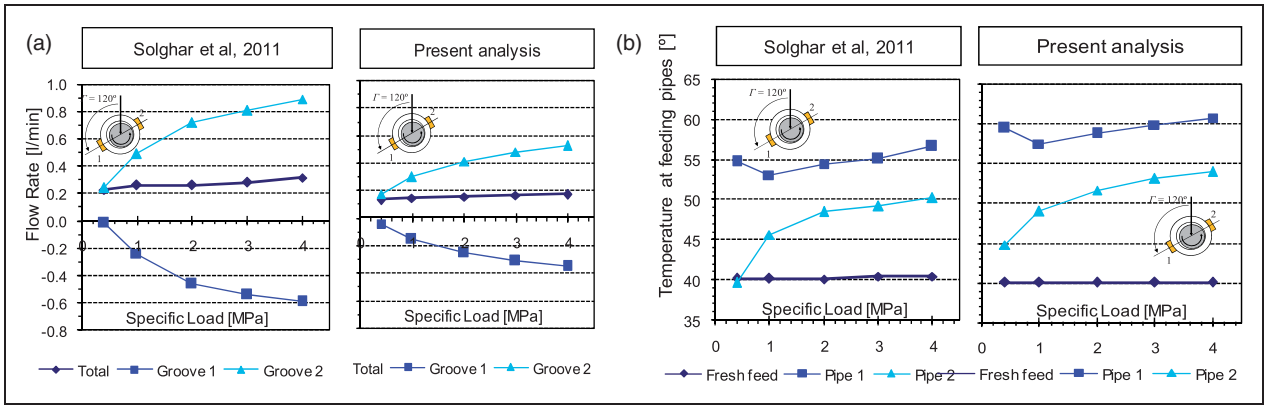

Figure 8. Comparison between experimental data published by the authors[9] and the present analysis for (a) flow rate and (b) temperature raise at feeding pipes due to negative feeding flow rate ($\Gamma = 120^\circ$).

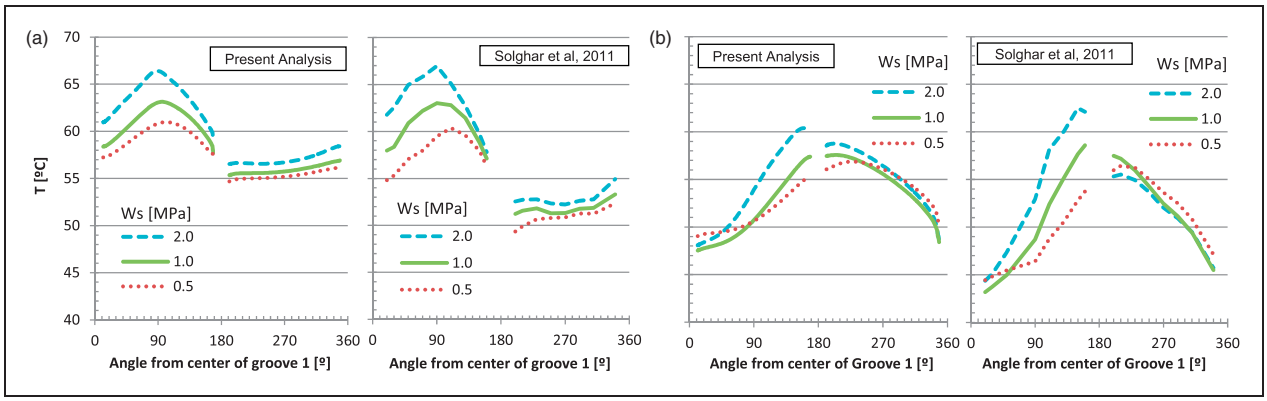

Figure 9. Comparison between experimental results published by the authors[9] and the present analysis for the temperature profile at the bush-film interface for (a) $\Gamma = 120^\circ$ and (b) $\Gamma = 60^\circ$.

the opposite groove due to mixing of hot refluxed oil with fresh oil inside the feeding pipes, governed by equation (23), was also quite satisfactorily predicted (Figure 8b).

The theory–experiment comparison concerning the temperature profile at the bush–film interface is presented in Figure 9(a,b) for two different load angles (60° and 120°, respectively). The trends have been fairly well predicted despite the disruptive phenomena present, such as the negative feeding flow rate present in one of the grooves. The slightly shallower temperature ranges predicted might be due to the underestimation of flow rate. Nevertheless, all predictions of maximum bush temperature (T_{max}) were within 2 °C of experimental measurements.

The underestimation of flow rate in the present model is, unfortunately, a common issue in many models and design tools when analysing the specific case of twin groove bearings.[1,17,22,38,42] The fact that many approaches often simply omit this kind of validation altogether might inclusively indicate that this problem may be even more common. This underestimation might be due to an intrinsic limitation of the modelling of grooves located within the ruptured film region (in twin groove plain journal bearings this always the case). In fact, the flow rate calculations are performed at groove edges using pressure gradients. These calculations might be limitative if performed near film rupture and reformation boundaries, where complex phenomena take place.[32,33,43] Nevertheless, it is interesting to note that the underestimation of flow rate does not seem to affect T_{max}, predicting only a slightly higher temperature level at the unloaded land of the bearing for high loads (see Figure 9a). It is interesting to know that a similar effect (same T_{max}, lower temperature level at unloaded region) may be experimentally obtained if flow rate is reduced (by decreasing feeding pressure), as observed experimentally by Brito et al.[5] So the theoretical under-prediction of flow rate and the experimental reduction of flow rate seem to have a similar, tenuous effect of thermal behaviour and the slight differences between theory and experiment observed in Figure 9(a) may be attributed to this under-prediction.

Results and discussion

The operating parameters and lubricant properties used in the analysis are presented in Tables 1 and 2.

Table 1. Geometric characteristics, operating and feeding conditions used in the analysis.

		Units	Default value/range
Geometric characteristics			
Inner bush diameter (nominal)	d	mm	100
Outer bush diameter	D	mm	200
Bush width/diameter ratio	b/d		0.8
Groove number			2
Groove angle with load line			30°–150°
Groove length/bush length ratio	a/b		0.875
Groove width/diam. ratio	w/d		0.18
Bearing radial clearance (at 20 °C)	C_r	μm	75
Operating and feeding conditions			
Rotational speed	N	r/min	3000
Specific load range (approx).	Ws	MPa	0.1–10
Oil feeding pressure	P_f	kPa	100
Oil feeding temperature	T_f	°C	40

Table 2. Lubricant properties used in the analysis.

Lubricant properties			Value
$T1$		°C	40
$T2$		°C	70
Dynamic viscosity at $T1$	μ_{T1}	Pa.s	0.0293
Dynamic viscosity at $T2$	μ_{T2}	Pa.s	0.0111
Specific heat	C_p	J/kg.K	2000
Density	ρ	kg/m^3	870
Thermal conductivity	k	W/mK	0.13

The angle between the plane of the axial groove centrelines and the load line, here designated simply as the groove angle or load angle, Γ, is measured in the direction of shaft rotation, as seen at the top right of Figure 10. This angle is normally 90° in twin axial groove journal bearings. However, it can assume other values, namely when there is permanent or temporary changes in the loading direction. The effect of Γ upon the hydrodynamic pressure field is presented in Figure 10 for a fixed specific load ($W_s = 0.6$ MPa) and five different values of Γ (30°, 60°, 90°, 120° and 150°). The groove locations are easily identifiable due to the constant pressure plateaus observable around circumferential coordinates 0° and 180°. The coordinate system for pressure and temperature fields are as defined in Figure 2.

It can be seen that Γ interferes substantially with the hydrodynamic pressure field under certain load angles. In fact, within grooves there is no relevant hydrodynamic pressure generation because no thin convergent film is present. The grooves are considered to be at a constant pressure (the feeding pressure, P_f) and they normally act as a pressure source. However, if the pressure in the vicinity is higher than P_f, then the groove will start acting as a pressure sink and the direction of the flow will be reversed. Under these conditions, the lubricant will flow from the bearing gap into the groove and out of the bearing through the feeding pipe. It can be seen that for Γ = 30° and 150°, the main pressure build-up zone was clearly located in the vicinity of grooves 2 and 1, respectively. These grooves interfere deeply with the hydrodynamic pressure generation. In order to compensate for this effect, the pressure level increases so that the same load can still be supported.

The effect of load angle on the hydrodynamic pressure field may be more easily quantified by observing in Figure 11(a) the pressure profiles at the midplane of the bearing for $Ws = 2$ MPa and by observing the variation of maximum hydrodynamic pressure for several values of specific load in Figure 11(b). It can be seen that lower peak pressures are obtained in the cases where the grooves have the least interference with the pressure field.

P_{max} may be regarded as a good indicator of the degree of interference of the grooves in the pressure field. It can be seen that at low loads P_{max} was minimized for load angles around 80°, which is close to the usual Γ value, 90°. At higher loads the minimum of P_{max} is deviated towards 60°. This might have to do with the fact that increasing load tends to reduce the attitude angle, and therefore the pressure build-up region will be located further upstream, farther from groove 2.

The worst cases were those with the lowest (30°) and the highest (150°) value of Γ, precisely those cases which displayed pressure build-up regions located closer to the feeding grooves. In fact, no convergence could be achieved for 30° tests with specific loads above 2 MPa due to excessive eccentricity. But bearing behaviour may be better understood by looking at the influence of Γ on total and partial flow rates (in each groove), displayed in Figure 12.

In line with previous findings by the authors,[6–8,44] it seems clear that the knowledge of the total flow rate by itself is insufficient to characterize the phenomena taking place inside the bearing gap. It is important to analyse what happens in each groove. The general trend found is that when Γ is increased, it tends to decrease the flow rate at groove 1 (upstream groove) and tends to increase the flow rate at groove 2 (downstream groove). Hot oil reflux (negative flow rate) can occur in both grooves (although, naturally, never simultaneously). This phenomenon happens even for low loads (see Figure 13a,b) when a groove is sufficiently close to the pressure build-up region and the local hydrodynamic pressure generated overcomes feeding pressure. In experimental works by the authors it was found that the increase of feeding pressure may reduce the magnitude of negative flow rate or even eliminate it if the pressure build-up region is not too close to a groove.[6,9] Eliminating this effect altogether might

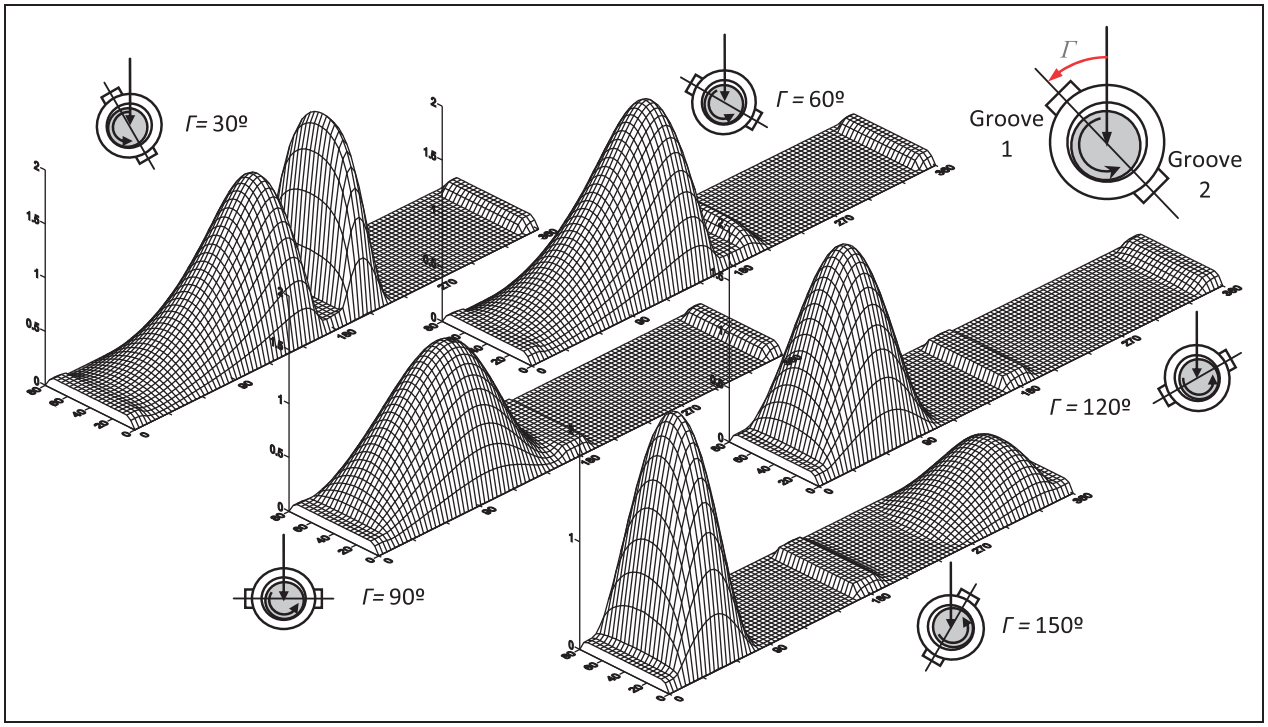

Figure 10. Influence of the location of the grooves with respect to the load line on the hydrodynamic pressure field ($Ws = 0.6$ MPa).

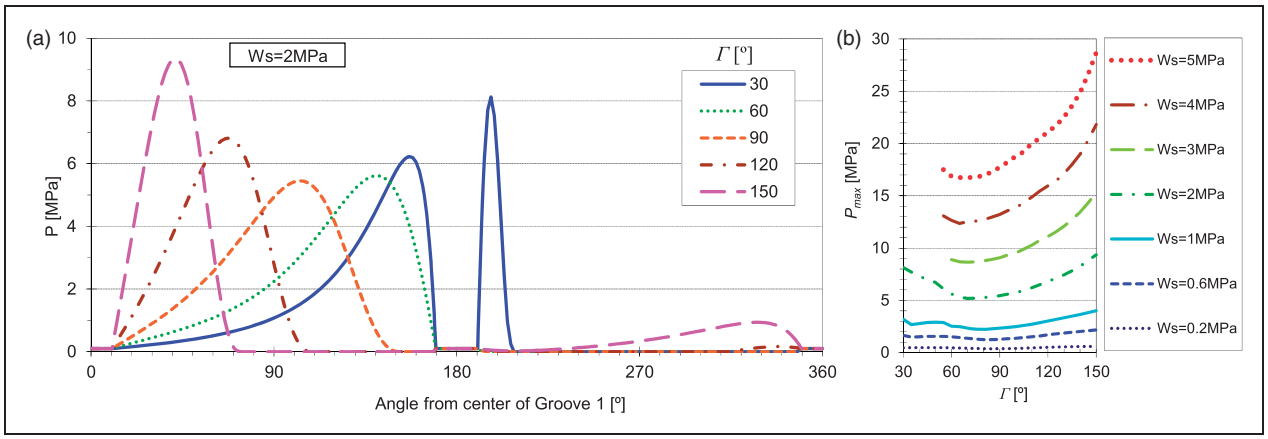

Figure 11. Influence of Γ on (a) the hydrodynamic pressure profile at the midplane of the bearing ($Ws = 2$ MPa) and (b) on the maximum hydrodynamic pressure, for several values of specific load.

require in some cases shutting off the groove or providing feeding pressures which are more typical of hydrostatic bearing applications. The flow rate trends are mainly explained by the relative magnitude of the pressure build-up region and its location relatively to each feeding groove. It is unclear why the decreasing trend of the flow rate in groove 1 is broken between 120° and 150° for the higher load range. The evolution of these flow rates with specific load can also be analysed for each value of Γ, as displayed in Figure 13.

It is interesting to analyse the totally different behaviour of flow rate at different groove angles and the relative weight of the flow rate in each groove for a given Γ value:

- In the case of the lowest Γ tests (30°), the flow rate at groove 1 is much higher than that at groove 2, which is always negative. This is so because the latter groove is right in the midst of the pressure build-up region.
- For $\Gamma = 60°$ the flow rate at groove 2 is only negative for W_s lower than 2 MPa. By increasing Γ this flow rate is always increasingly positive, while the flow rate at groove 1 is increasingly negative.

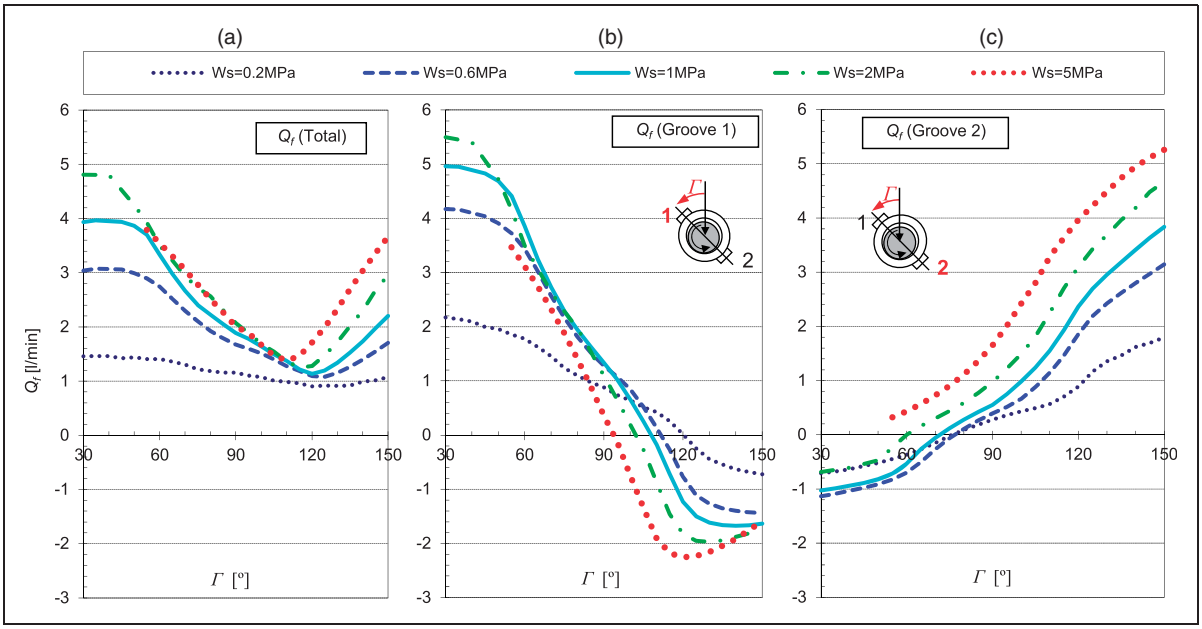

Figure 12. Influence of Γ on (a) total flow rate, (b) flow rate in groove 1 and (c) flow rate in groove 2.

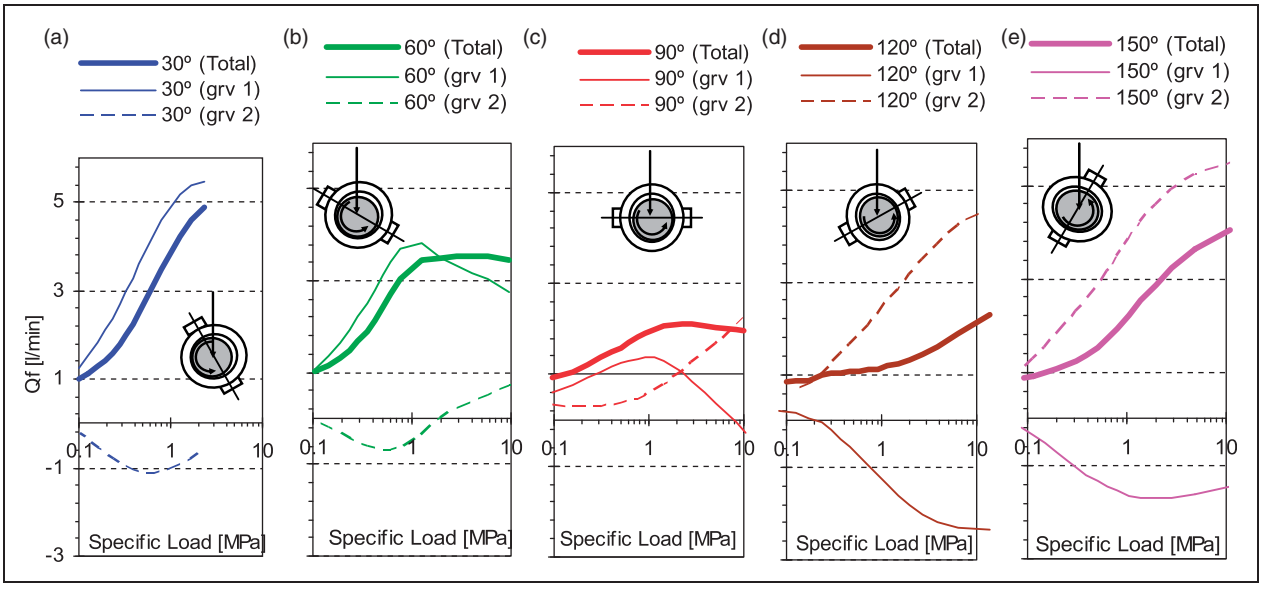

Figure 13. Total flow rate and partial flow rates in each groove for (a) Γ = 30°, (b) Γ = 60°, (c) Γ = 90°, (d) Γ = 120° and (e) Γ = 150°.

– For Γ = 90° (the usual value) the partial flow rates are equilibrated. However, oil reflux would appear for specific loads above 8 MPa (although such high loads are unlikely to occur in practice). This is an undesirable situation because the very high eccentricities present could risk the safety of the bearing.
– For Γ = 120° and 150° the flow rate in groove 1 is negative for nearly the whole load range. This constitutes the least desirable situation, because oil is being retrieved from the bearing gap instead of being fed to it, just upstream of the region where it would be most needed – the active land of the bearing and more precisely, the minimum film thickness region. Under high eccentricities this could even induce bearing seizure (although the present model is not able to deal with contact-related phenomena).

One of the consequences of hot oil reflux from one of the grooves is the effective rise of the feeding temperature in the opposite groove, as already depicted in Figure 6. In fact, the hot oil flowing out of the bearing gap through a groove mounts up the feeding pipes, then mixes with the fresh oil feeding (which is at a temperature T_f) and is re-fed to the opposite groove at a temperature which is actually higher than T_f.

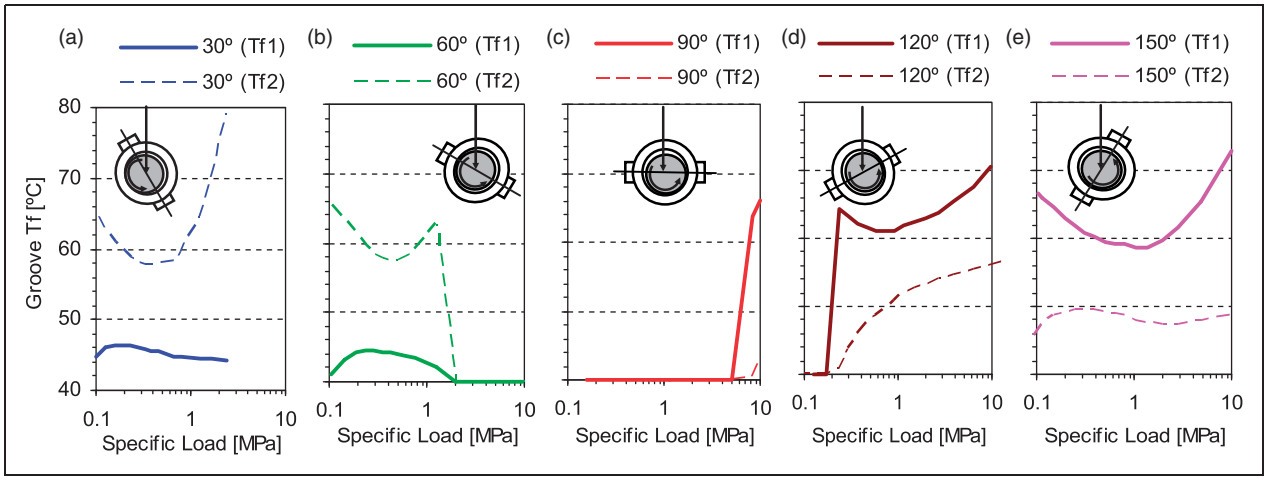

Figure 14. Influence of negative flow rate in one of the grooves, on the effective feeding temperature of the opposite groove, for (a) $\Gamma = 30^\circ$, (b) $\Gamma = 60^\circ$, (c) $\Gamma = 90^\circ$, (d) $\Gamma = 120^\circ$ and (e) $\Gamma = 150^\circ$. For each case, highest level curves denote the temperature of the hot oil reflux, while the lower level curves denote the temperature at which this hot oil is being re-supplied to the opposite groove after mixing with fresh feeding oil. When no reflux is present, both values are equal to T_f.

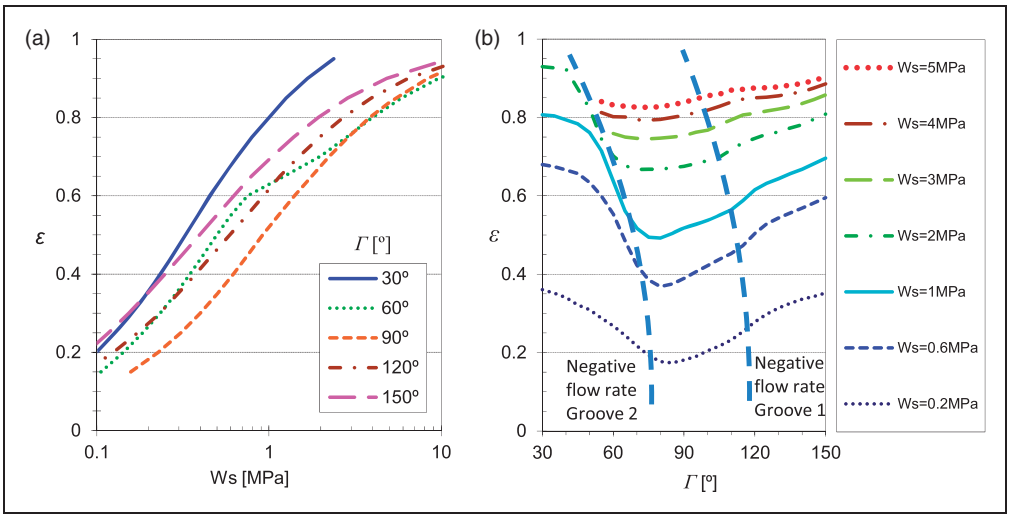

Figure 15. Influence of Γ in eccentricity ratio, (a) represented as a function of specific load for several values of Γ and (b) represented as a function of Γ for several values of specific load.

The incorporation of this effect into the analysis, notably through equation (23), is one of the novelties proposed in the present work.

The temperature of the hot oil reflux (higher temperature curve) and its effect upon the feeding temperature at the opposite groove (lower temperature curve) can be observed in Figure 14. Comparing these charts with the flow rate charts presented before in Figure 13, it can be confirmed that when no reflux is present, both values are equal to T_f (40 °C). The actual temperature of the oil supplied to the positive flow rate groove will depend not only on the temperature of the hot oil reflux but also on the value of the flow rates.

The influence of Γ on eccentricity ratio is displayed in Figure 15. It has some parallel with the maximum pressure chart (Figure 11b). Again, the highest values are obtained with the most extreme values of Γ (30° and 150°). The lowest Γ seems to be especially deleterious for this parameter. The 60° tests also display an abnormal eccentricity but only within the lower, less dangerous, range of eccentricity. On the contrary, they display the best performance (lowest eccentricity) for the higher load range, even better than that for the 90° case. The reason for this resides in the fact that the increase of load pushes the pressure build-up region upstream, away from groove 2. Under these conditions, the hydrodynamic pressure generation is less hampered by the presence of grooves and so eccentricity is minimized.

It is also helpful to observe the variation of eccentricity as a direct function of Γ (Figure 15b). Threshold (dotted) lines may be identified, where the flow rate in a groove crosses zero (recall Figure 12c).

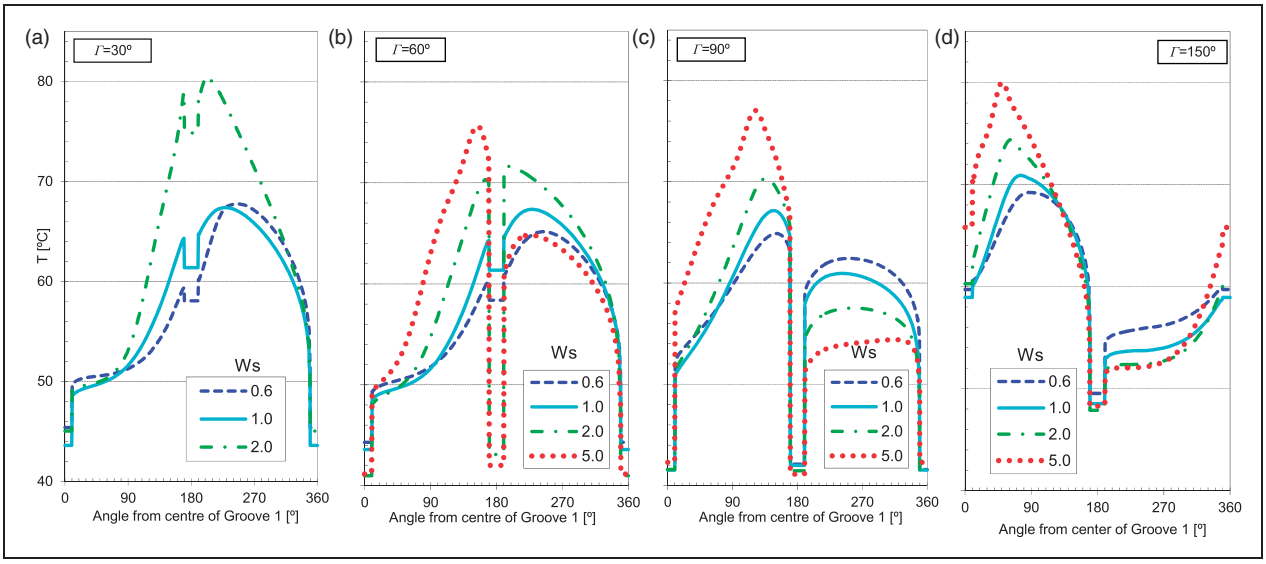

Figure 16. Influence of Γ on the temperature profile at the midplane of the inner bush surface for (a) $\Gamma = 30^\circ$, (b) $\Gamma = 60^\circ$, (c) $\Gamma = 90^\circ$ and (d) $\Gamma = 150^\circ$.

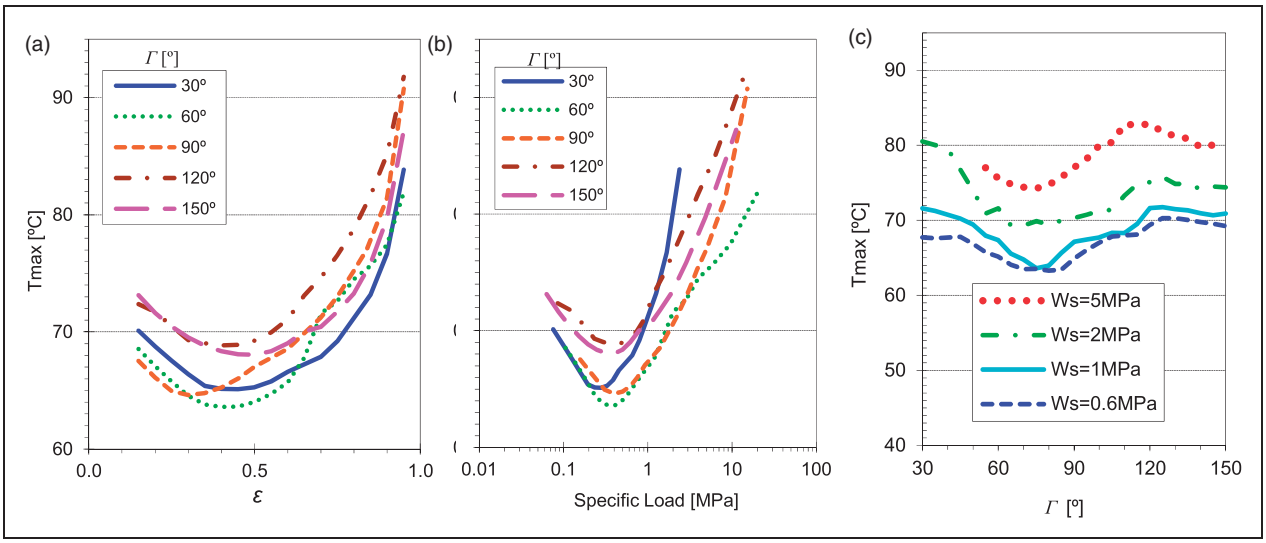

Figure 17. Influence of Γ in maximum temperature, (a) represented as a function of eccentricity for several values of Γ, (b) represented as a function of specific load for several values of Γ and (c) represented as a function of Γ for several values of specific load.

It seems clear that the occurrence of negative flow rate in groove 2 deeply affects eccentricity. In fact, eccentricity is minimum close to this threshold but starts increasing sharply when entering in the negative flow rate region (when Γ is decreased). For the higher load curves (3 MPa and above) it was not even possible to attain convergence for $\Gamma < 60^\circ$ precisely due to the sharp increase of the eccentricity with lower values of Γ (below the threshold line). On the other hand, a less pronounced increase of the eccentricity may be detected when exceeding the Γ threshold value for the inception of negative flow rate at groove 1. This does not mean that this increase is innocuous, because in the high load cases the already high eccentricity is amplified in 0.05 between the lowest and the highest value. In practical applications, variations of this magnitude in heavily loaded bearings might well be sufficient to induce contact.

The influence of Γ on the temperature profiles at the bush–film interface is presented in Figure 16. The following observations may be pointed out:

- The diverse cooling effect of each groove is in line with the corresponding flow rate (Figure 12).
- The circumferential location of the maximum bush temperature depends not only on the angle of the load (this is straightforward) but also on its magnitude. This is so because the higher the load, the lower will be the attitude angle. As a consequence, the circumferential coordinate of the minimum film

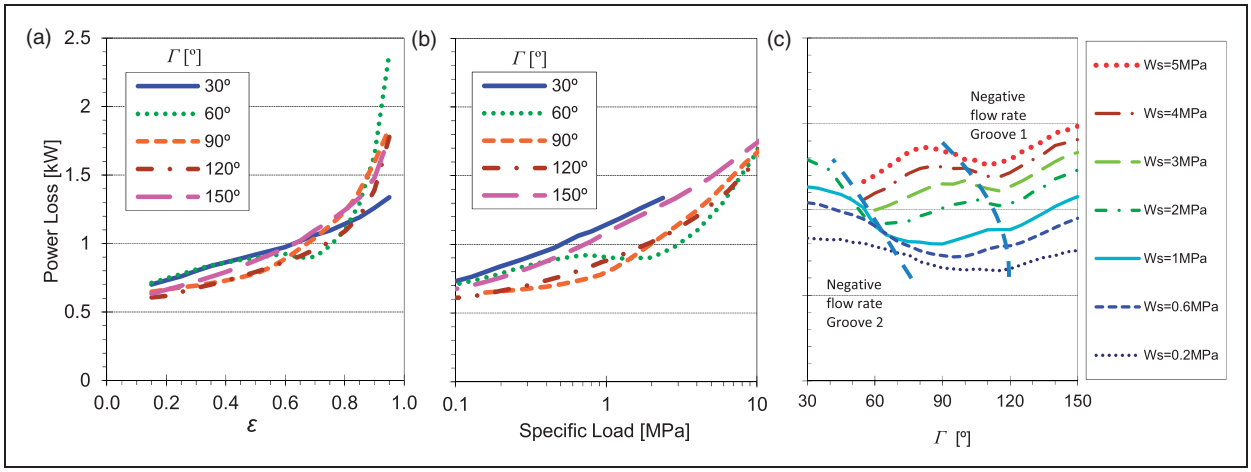

Figure 18. Influence of Γ in power loss, (a) represented as a function of eccentricity for several values of Γ, (b) represented as a function of specific load for several values of Γ and (c) represented as a function of Γ for several values of specific load.

thickness location (and therefore the bulk of the viscous dissipation) will be located further upstream.

- The cases where oil reflux occurred in one of the grooves are easily recognizable because the temperature at the corresponding groove is very high and there is no temperature decrease across the groove. In these cases, the general temperature level is also higher than that of the cases where no oil reflux occurred. This can be observed, for instance, by comparing the profiles of the 90° cases (Figure 16c), where no hot oil reflux occurred, against the 150° cases (Figure 16d), where hot oil reflux was always present at groove 1.
- It can be seen that for 2 MPa the 30° test displays a much higher temperature than the others. This is in accordance with the excess in eccentricity detected for this case (Figure 15b). Actually, the differences in the temperature levels in the cases tested with this specific load are closely related to the differences detected in eccentricity.

The influence of Γ in maximum temperature is presented in Figure 17 in three different ways. When presenting T_{max} as a function of eccentricity (Figure 17a), there are no substantial differences between curves, but of course, this can be deceiving, as a given eccentricity corresponds to very dissimilar load capacities, depending on the value of Γ.

When analyzing T_{max} as a function of specific load (Figure 17b) it can be seen that above 1 MPa the worst choices for Γ in terms of T_{max} are 30°, then 120°, then 150°. According to this chart, T_{max} is minimized by load angles 60° and 90°, depending on the load range. However, by observing Figure 17(c), which displays T_{max} as a direct function of Γ, it can be seen that the optimum value is actually located somewhere between 70° and 80°. This is precisely the same range which also minimizes eccentricity (Figure 15b). This region also coincides with the range where the groove 2 flow rate is small but still positive (Figure 12c).

Concerning power loss, it seems useful also to show the evolution of this parameter with eccentricity and load. It seems (see Figure 18a) that T_{max} is mainly a function of ε, with relatively small differences on power loss when varying Γ for a given ε. However, it is also important to analyse this parameter as a function of the specific load (Figure 18b). It can be seen that the most extreme values of Γ (30° and 150°) yield the highest power losses obtained. This is because these cases also displayed the highest eccentricity for a given load (see Figure 15b). According to this chart, the groove angles which optimize power loss are again 90° ($W_s < 1.5$ MPa) and 60° (1.5 MPa $< W_s <$ 6 MPa).

The same power loss results presented as a direct function of Γ (Figure 18c) also highlight the influence of negative flow rate. For high loads the lowest power loss is obtained when the flow rate in groove 2 is close to the threshold of being negative. But when in fact it turns negative there is a sharp rise of the power loss. There is also a local minimum close to the region where the flow rate in groove 1 is zero or even slightly negative. If Γ is further increased, then the power loss starts increasing steadily.

Conclusions

A THD model has been proposed and used to assess the behaviour of twin axial groove hydrodynamic journal bearings subjected to varying load angle, Γ (the angle between the load line and the plane defined by the midline of the grooves). The model is based on the simultaneous solution of the GRE through a mass conserving algorithm and the energy equation within the fluid domain, as well as the Laplace equation within the solid domain.

Realistic lubricant feeding conditions, namely the actual dimensions of feeding grooves, have been incorporated into the analysis, while energy-conservative models for the ruptured film region and for the lubricant mixing at the grooves, have been proposed. This included the first full modelling of the effect of negative flow rate in a groove, a phenomenon originally described experimentally in detail by the authors in previous publications.

The model was successfully validated, with the results obtained appearing to be globally coherent, physically plausible and with small randomness. The robustness of the model was confirmed for a wide range of specific load (0.1–10 MPa) and load angle (30°–150°).

Γ was found to affect significantly most of the performance parameters. This had mainly to do with the interference of axial grooves in the hydrodynamic pressure generation. When in the vicinity of pressure build-up regions, the grooves act as pressure sinks, deeply affecting the shape of the pressure profiles, the eccentricity, the feeding flow rates and eventually the whole thermal behaviour of the bearing.

The analysis of what is actually happening separately in each groove was vital in order to understand the bearing behaviour. In fact, the feeding flow rate in each groove varies with both the load magnitude and the load angle. Frequently, the flow rate in one of the grooves became negative (hot oil reflux), with the hot refluxed lubricant getting out of the bearing through the feeding pipes, mixing with the fresh lubricant before being re-fed to the opposite groove at a temperature which is substantially higher than the feeding temperature.

Eccentricity ratio, maximum bush temperature and power loss were found to be minimized for Γ values in the range of 70°–80°, depending on load. This usually happened when the flow rate at the groove located downstream of the active region of the bearing (groove 2) was low and close to being negative. However, a rapid deterioration of bearing performance was observed once lower Γ values started inducing negative flow rates in this groove. Increases in eccentricity ratio, power loss and maximum bush temperature as high as 50%, 40% and 20%, respectively, were predicted under these conditions. Also, the bearing performance was found to strongly deteriorate with extreme load angles of 30° and 150°. It seems clear that the location of axial grooves should be such that it does not interfere with the hydrodynamic pressure profile. The analysis performed in the present work highlights the importance of realistically treating the feeding conditions in bearing design tools. In fact, a suitable tuning of these conditions might indeed be able to contribute, in ways that conventional bearing design tools do not anticipate, for substantial savings in operating cost and in the safe operation of journal bearings.

Funding

This work was supported by Fundacao para a Ciencia e a Tecnologia/EU-FEDER (Project POCTI/EME/39202/2001); and by MCTES-FCT/POPH-QREN (PhD grant SFRH/BD/22278/2005 and Postdoctoral grant SFRH/BPD/89553/2012).

Conflict of interest

None declared.

References

1. Claro JCP and Miranda AS. Analysis of hydrodynamic journal bearings considering lubricant supply conditions. *Proc IMechE Part C: J Mechanical Engineering Science* 1993; 207: 93–101.
2. Costa L, Miranda AS, Fillon M, et al. An analysis of the influence of oil supply conditions on the thermohydrodynamic performance of a single groove journal bearing. *Proc IMechE Part J: J Engineering Tribology* 2003; 217: 133–144.
3. Brito FP, Fillon M, Miranda AS, et al. The role of lubricant feeding conditions on the performance improvement and friction reduction of journal bearings. *Tribol Int* 2014; 72: 65–82.
4. Costa L, Fillon M, Miranda AS, et al. An experimental investigation of the effect of groove location and supply pressure on the THD performance of a steadily loaded journal bearing. *ASME J Tribol* 2003; 122: 227–232.
5. Brito FP, Bouyer J, Fillon M, et al. Experimental investigation of the influence of supply temperature and supply pressure on the performance of a two axial groove hydrodynamic journal bearing. *ASME J Tribol* 2007; 129: 98–105.
6. Brito FP, Miranda AS, Claro JCP, et al. The role of each groove on the behavior of twin axial groove journal bearings. In: *IBERTRIB – Congreso Ibérico de Tribología, Escuela de Ingenieros*, Bilbau, 20–21 June 2007, CD-ROM.
7. Brito FP, Miranda AS, Claro JCP, et al. The role of lubricant supply temperature on the performance of twin groove journal bearings: an experimental study. *Int J Surface Sci Eng* 2011; 5(4): 286–299.
8. Brito FP, Miranda AS, Claro JCP, et al. Experimental comparison of the performance of a journal bearing with a single and a twin axial groove configuration. *Tribol Int* 2012; 54: 1–8.
9. Arab Solghar A, Brito FP, Claro JCP, et al. An experimental study of the influence of loading direction on the thermohydrodynamic behavior of twin axial groove journal bearing. *Proc IMechE Part J: J Engineering Tribology* 2011; 225(5): 245–254.
10. Dowson D, Taylor CM and Miranda AS. The prediction of liquid film journal bearing performance with a consideration of lubricant film reformation, part I and II. *Proc IMechE Part J: J Engineering Tribology* 1985; 119(C2): 95–102102–111.
11. Braun MJ and Hannon WM. Cavitation formation and modelling for fluid film bearings: a review. *Proc IMechE Part J: J Engineering Tribology* 2010; 224(9): 839–863.
12. Chun S and Lalas D. Parametric study of inlet oil temperature of a half-circumferential grooved journal bearing. *STLE Tribol Trans* 1992; 35: 213–224.

13. Boncompain R, Fillon M and Frêne J. Analysis of thermal effects in hydrodynamic bearings. *ASME J Tribol* 1986; 108: 219–224.
14. Knight JD and Ghadimi P. Effects of modified effective length models of the rupture zone on the analysis of a fluid journal bearings. *STLE Tribol Trans* 1992; 35: 29–36.
15. Rajalingham C and Prabhu BS. The influence of variation of viscosity with temperature on the steady state characteristics of journal bearings – simple analysis. *Tribol Int* 1987; 20(5): 261–266.
16. Pierre I and Fillon M. Influence of geometric parameters and operating conditions on the thermohydrodynamic behavior of plain journal bearings. *Proc IMechE Part J: J Engineering Tribology* 2000; 214: 445–457.
17. EI-Deihi MKI and Gethin DT. A thermohydrodynamic analysis of a twin axial groove bearing under different loading directions and comparison with experiment. *ASME J Tribol* 1992; 114: 304–310.
18. Tanaka M. Recent thermohydrodynamic analyses and designs of thick-film bearings. *Proc IMechE Part J: J Engineering Tribology* 2000; 214: 107–122.
19. Khonsari MM. A review of thermal effects in hydrodynamic bearings. Part II. *J Bear ASLE Trans* 1987; 30(1): 26–33.
20. Basri H and Neal PB. Oil flow in axial groove journal bearings. In: *Proceedings of the seminar on developments in plain bearings for the '90s, IMechE Tribology Group*. London: Mechanical Engineering Publications, 1990, pp.11–17.
21. Gethin DT and EI-Deihi MKI. Effect of loading direction on the performance of a twin-axial groove cylindrical-bore bearing. *Tribol Int* 1987; 20(4): 179–185.
22. Gethin DT and El-Deihi MKI. Thermal behavior of a twin axial groove bearing under varying loading direction. *Proc IMechE Part C: J Mechanical Engineering Science* 1990; 204: 77–90.
23. Roy L and Laha SK. Steady state and dynamic characteristics of axial grooved journal bearings. *Tribol Int* 2009; 42: 754–761.
24. Roy L. Thermo-hydrodynamic performance of grooved oil journal bearing. *Tribol Int* 2009; 42: 1187–1198.
25. Brito FP. *Thermohydrodynamic performance of twin groove journal bearings considering realistic lubricant supply conditions: an experimental and theoretical study*. PhD Thesis, School of Engineering, Universidade do Minho, Guimarães, Portugal, http://repositorium.sdum.uminho.pt/handle/1822/9884.
26. Pinkus O. *Thermal aspects of fluid film tribology*. New York: ASME Press, 1990.
27. Elrod HG. A cavitation algorithm. *ASME J Lubr Technol* 1981; 103(3): 350–354.
28. Fitzgerald MK and Neal PB. Temperature distributions and heat transfer in journal bearings. *ASME J Tribol* 1992; 114: 122–130.
29. Ferron J, Frêne J and Boncompain R. A study of the thermohydrodynamic performance of a plain journal bearing. Comparison between theory and experiments. *ASME J Lubr Technol* 1983; 105: 422–428.
30. Pierre I and Fillon M. Validity limit of the two-dimensional thermohydrodynamic analysis of plain journal bearings. In: *Proceedings of the international tribology conference*, ITC 2000, Nagasaki, Japan, 29 October–2 November 2000, Japanese Society of Tribologists, vol. III, pp.1555–1560.
31. Frêne J, Nicolas D, Degueurce B, et al. Lubrification hydrodynamique – paliers et butées. *Collection de la direction des Études et Recherches d'Électricité de France*. Paris: 72, Editions Eyrolles, 1990, pp.354–358.
32. Heshmat H. The mechanism of cavitation in hydrodynamic lubrication. *Tribol Trans* 1991; 34(2): 177–186.
33. Knight JD and Ghadimi P. Analysis and observation of cavities in a journal bearing considering flow continuity. *STLE Tribol Trans* 2001; 44: 88–96.
34. Kosasih PB and Tieu AK. An investigation into the thermal mixing in journal bearings. *Proc IMechE Part J: J Engineering Tribology* 2004; 218: 379–389.
35. Jeddi L, El Khlifi M and Bonneau D. Thermohydrodynamic analysis for a hydrodynamic journal bearing groove. *Proc IMechE Part J: J Engineering Tribology* 2005; 219: 263–274.
36. Dowson D, Hudson J, Hunter B, et al. An experimental investigation of the thermal equilibrium of steadily loaded journal bearings. *Proc IMechE Part B: J Engineering Manufacture* 1966–67; 101: 70–80.
37. Andrisano AO. An experimental investigation on rotating journal surface temperature distribution. *ASME J Tribol* 1988; 110: 638–645.
38. Ma MT and Taylor CM. A theoretical and experimental study of thermal effects in a plain circular steadily loaded journal bearing. In: *IMechE seminar: plain bearings – energy efficiency and design, mech. engs*. London: Publications Ltd, 1992.
39. Jang JY and Khonsari MM. Design of bearings on the basis of thermohydrodynamic analysis. *Proc IMechE Part J: J Engineering Tribology* 2004; 218: 355–363.
40. Pierre I, Bouyer J and Fillon M. Thermohydrodynamic behavior of misaligned plain journal bearings: theoretical and experimental approaches. *Tribol Trans* 2004; 47(4): 594–604.
41. Brito FP, Bouyer J, Fillon M, et al. Experimental investigation on the thermal behavior and performance characteristics of a twin axial groove journal bearing as a function of applied load and rotational speed. In: *5th international conference on mechanics & materials in design – M2D'2006*, symposium on wear and lubrication in design, FEUP, Porto, 24–26 July 2006. CD-ROM (ISBN 972-8826-10-9).
42. Engineering Science Data Unit, ESDU. *ESDU item no. 84031. Calculation methods for steadily loaded axial groove hydrodynamic journal bearings*. London: Engineering Sciences Data Unit (ESDU) International Plc, 1984.
43. Groper M and Etsion I. Reverse flow as a possible mechanism for cavitation pressure build-up in a submerged journal bearing. *ASME J Tribol* 2002; 124: 320–326.
44. Brito FP, Miranda AS, Claro JCP, et al. On the occurrence of negative groove flow rate in twin groove hydrodynamic journal bearings. In: *15th international conference on experimental mechanics (ICEM15)*, FEUP, Porto, Portugal, 22–27 July 2012 (extended abstract), pp.875, 876.